energies

MDPI

Article

# Experimental and Simulation Studies of Strength and Fracture Behaviors of Wind Turbine Bearing Steel Processed by High Pressure Torsion

**Ning Wang [1,2,*], Luis V. Wilches Peña [2], Ling Wang [2], B. G. Mellor [3] and Yi Huang [3]**

1 Key Laboratory of Pressure Systems and Safety, Ministry of Education, East China University of Science and Technology, 200237 Shanghai, China

2 National Center for Advanced Tribology at Southampton (NCATS), University of Southampton, Southampton SO17 1BJ, UK; lvwp1e14@soton.ac.uk (L.V.W.P.); ling.wang@soton.ac.uk (L.W.)

3 Materials Research Group, Faculty of Engineering and the Environment, University of Southampton, Southampton SO17 1BJ, UK; b.g.mellor@soton.ac.uk (B.G.M.); y.huang@soton.ac.uk (Y.H.)

* Correspondence: nwang@ecust.edu.cn or nw1r14@soton.ac.uk; Tel.: +86-21-6425-3513

Academic Editor: Frede Blaabjerg

Received: 3 November 2016; Accepted: 2 December 2016; Published: 8 December 2016

**Abstract:** White structure flaking (WSF) has been found to be one of the failure modes in bearing steels under rolling contacts through the formation of cracks associated with a microstructural change called white etching area (WEA). In the present research, the effects of the high-pressure torsion (HPT) process on the microstructure and mechanical properties of an AISI 52100 alloy are studied. An annealed AISI 52100 was subjected to high-pressure torsion at room temperature under a pressure of up to ~6 GPa for up to three turns. Finite-element modeling (FEM) was used to simulate the process under high-pressure torsion and quasi-constrained conditions to reveal the material property changes occurring in HPT. Scanning electron microscopy and microhardness testing after processing were used to investigate the microstructural and mechanical property evolution of the steel. Strain induced microstructural transformations occur and affect the mechanical properties in a similar way to the well-known white etching area (WEA) found beneath the surface of wind turbine bearings. Here, HPT is used to study the feasibility of creating microstructural changes that are similar to WEA. This paper presents the preliminary results of using HPT to produce WEAs.

**Keywords:** high pressure torsion (HPT); microstructure; mechanical properties; white etching area (WEA)

## 1. Introduction

Bearing steels have been widely used for over 100 years in various applications. White structure flaking (WSF) is a damage mechanism responsible for a large amount of failures of bearings in wind turbine gearboxes [1]. WSF is related to microstructural changes registered close to the contact zones called white etching areas (WEAs) [2]. WEAs in AISI 52100 consist of carbon saturated nanograins of ferrite, which vary in sizes in the 10–100 nm range [3]. It has been suggested that WEAs form in a region of localized high plastic deformation, as a consequence of the presence of a high dislocation density, low temperature recrystallization and high carbon dissolution from the cementite into the ferritic matrix. WEAs are found to be associated with micro cracks (White Etching Cracks or WECs). However, the nature and relationships between WEA and micro-cracks are not completely understood [4].

It is commonly observed that crystalline materials undergo grain refinement at nano scales under severe plastic deformation (SPD) [5], such as in the high pressure torsion (HPT) process [6]. High pressure torsion (HPT) is an efficient way to obtain and reproduce a well-defined deformation history in small samples through controlled pressure and speed [7].

Finite-element modeling (FEM) analysis has been used to study the evolution of plastic deformation in metals under HPT: alloys investigated include the magnesium alloy AZ31 [8] and copper [9]. In addition, similar phenomena related to WEA formation have been reported in steels by using HPT [6]. The nanostructure and the phase composition of a UIC 860V pearlitic steel deformed by high-pressure torsion has been studied. The strain induced dissolution of cementite led to the formation of nanostructure in three stages. In the second stage, the cementite begins to be dissolved and forms a WEA, similar to that observed on the surface of railroad tracks.

The aim of this work is to gain a better understanding of the behavior and microstructural evolution of AISI 52100 bearing steel during a shear deformation under high hydrostatic pressure, in particular to study the mechanism responsible for WEA development. The results of this analysis will be expected to help guide the development of lasting solutions to a pressing problem in wind turbine gearboxes.

## 2. Experiments and Modeling Procedures

### *2.1. Materials and High Pressure Torsion (HPT) Test Sample Preparation*

Standard rollers of AISI 52100 bearing steel were used in this study and the chemical composition and mechanical properties of the roller material are shown in Tables 1 and 2, respectively. The as-received material was in the form of cylindrical rods 10 mm in diameter and 14 mm long with hardness of 750 HV (quenched + tempered condition). In order to process the bearing steel using the HPT test machine available at the University of Southampton, the rollers were softened by annealing at 820 °C for 6 h followed by cooling to 700 °C at 10 °C per hour and finally cooled in air to room temperature. The hardness of the annealed material was 180 HV. Sample discs of 10 mm diameter and ~0.86 mm thickness were obtained by slicing the annealed rollers.

**Table 1.** The chemical composition (wt %) limits for AISI 52100.

| C | Mn | Si | P | S | Cr | Mo | Fe |
|---|---|---|---|---|---|---|---|
| 0.98–1.10 | 0.25–0.45 | 0.15–0.35 | 0.025max | 0.025max | 1.30–1.60 | 0.00–0.10 | balance |

**Table 2.** Mechanical properties of AISI 52100 [10].

| Ultimate Tensile Strength (Mpa) | Yield Strength (Mpa) | Vickers Hardness (HV) | Elastic Modulus (GPa) | Elongation |
|---|---|---|---|---|
| 2150–2450 | 1400–2200 | 750–850 | 190–210 | 5% |

The HPT processing was conducted under quasi-constrained conditions using a facility consisting of an upper and a lower anvil having central depressions with a diameter of 10 mm and depth of 0.25 mm, shown in Figure 1. The processing was carried out at ambient temperature by turning the lower anvil with a speed of 1 rpm under a given load of up to 470,000 N, equivalent to a pressure of up to 6.0 GPa. Tests were conducted on the discs subject to rotations of N = 1, 2 and 3 turns. The upper surface of each disc was marked immediately after HPT and prior to any microstructural analysis and hardness measurements. After HPT tests, the samples were polished and etched with 2% Nital and Villella's reagent in order to examine the microstructural changes in the material after different numbers of turns.

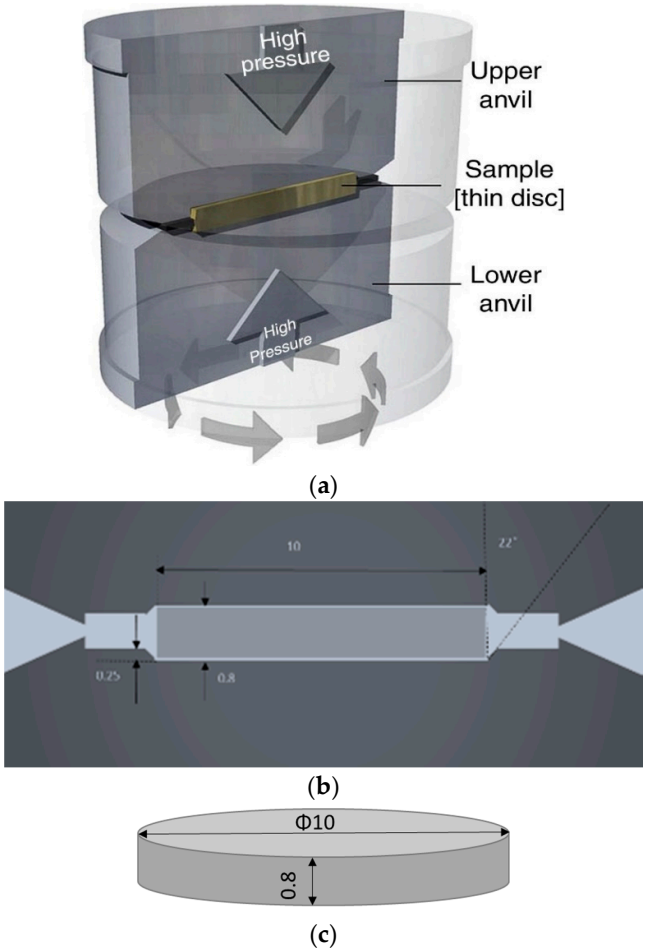


**Figure 1.** High pressure torsion (HPT) process with a hydrostatic pressure and torsional stress applied to the sample disc [11]. (**a**) A schematic of the HPT rig; (**b**) A disc sample held in the anvils; (**c**) A disc sample.

### 2.2. Finite Element Modelling

Using the 3D DEFORM software (v6.1, Scientific Forming Technology Corporation, Columbus, OH, USA) to simulate the HPT process is a very effective method. The dimensions of the anvils were specified to simulate the edge constraint condition. The anvils were regarded as rigid cylinders with a diameter of 50 mm and height of 20 mm. On the opposite faces of each anvil, there is a depression with a diameter of 10 mm and a depth of 0.25 mm. The sidewalls of the depression have an inclination angle of 22°, as is shown in Figure 1. The HPT specimens were modeled as rigid plastic elements with a diameter of 10 mm and a thickness of 0.8 mm.

During the simulation, an axial force in the range between 78,600 and 471,600 N was applied to the top anvil to simulate theoretical pressures in the range of 1.0 to 6.0 GPa. The lower anvil was forced to rotate at a constant rotational speed of 1 rpm without any movement in the axial direction. The contact between the bottom of the anvil depressions and the disc surfaces were defined in the software as "stick", preventing any slip of the samples [12].

### 2.3. Microhardness and Microstructure Observation

After the HPT tests, the samples were mounted and metallographically prepared. The hardness distribution across a radius of each sample was measured using a Matzusawa Seiki MHT-1 microhardness (Matsusawa Seiki Co. Ltd., Tokyo, Japan) instrument with a Vickers indenter using a load of 100 gf with a dwell time of 15 s. The microhardness value appropriate to each radial position was obtained

from the average of four separate hardness measurements recorded at points uniformly displaced around the selected position.

Moreover, the samples were etched using 2% Nital and Vilella's reagent and examined using Light Microscopy (LM) with an Olympus BX51 optical microscope (Olympus Co. Ltd., Tokyo, Japan), and JEOL JSM-6500F (JEOL Ltd., Tokyo, Japan) Scanning Electron Microscopy (SEM). All SEM images were taken using Secondary Electron Images (SEI).

## 3. Results

### *3.1. Simulation Results*

#### 3.1.1. The Distribution of the Effective Strain in High Pressure Torsion (HPT) Discs

Finite element simulations showed that plastic deformation occurred in a steady-state way. Actually, the simulation indicated that the only change in steady-state torsional plastic flow is related to the gradual outflow of the edge material around the disc between the two anvils. This pattern of extrusion or outflow, commonly referred to as "flash", reduced the thickness of the sample during the process.

As anticipated, the simulations show the effective strains imposed on the sample are lowest in the disc centers and highest at the edges. Figure 2 shows distributions of the effective strain on half of the top surfaces when $P$ = 3.0 GPa after 1/4, 1/2, 1 turn. It can be seen that the level of the effective strain is dependent upon the amount of rotation imposed on the sample. Lower levels of strain are observed near the center, and there is an essentially linear increase in strain away from the center. It is important to note that several remeshing steps took place during these simulations, and the new elements then acquire an average effective strain from the previous elements at the same location. Therefore, the occurrence of a large number of remeshing steps leads to an attenuation in the distribution of strain in areas having pronounced differences in the strain level. This explains the high level and curved distributions of strain near the centers of the samples after large rotations. Figure 3 shows the distributions of the effective strains in the cross-sections over one-half of the top surfaces for simulations with a 1/2 turn with pressures from 1 to 6 GPa. It is observed that the distributions of strain are relatively similar for each simulation. It is evident that variations in pressure had no significant influence on the distributions of the effective strains. This just agrees with the theoretical prediction of the effective strain, $\varepsilon$, given by an expression of the form:

$$\varepsilon = \frac{\theta r}{h\sqrt{3}} \tag{1}$$

where $\theta$ is the rotation angle, $r$ is the radial distance to the disc center and $h$ is the thickness (or height) of the disc.

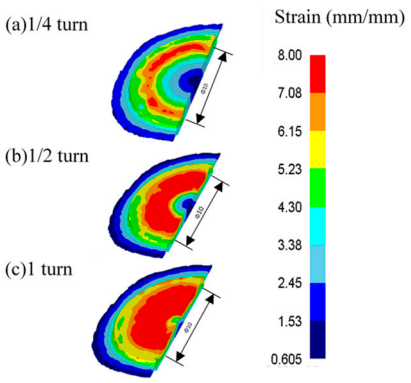


**Figure 2.** Distribution of strain on the half-disc surfaces and along the disc longitudinal sections for samples with (**a**) 1/4 turn; (**b**) 1/2 turn; and (**c**) 1 turn.

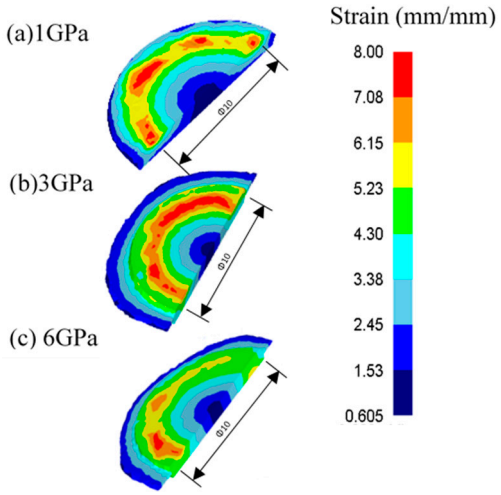


**Figure 3.** Distribution of strain on the half-disc surfaces and along the disc longitudinal sections of samples after a 1/2 turn with (**a**) 1 GPa; (**b**) 3 GPa; and (**c**) 6 GPa.

The transient distribution of the strain rate well explains the plastic flow due to deformation occurring under steady-state conditions, since the plastic deformation is only related to the cumulative time of deformation. Figure 4 illustrates the distribution of strain rate in samples treated under different given pressures of (a) 1, (b) 3 and (c) 6 GPa. It is readily apparent that, as anticipated, an increasing pressure increases the material outflow between the anvils, which produces a greater flash width. The manner of flow also changes because the plastic flow concentration occurs near the surface of the sample edge when processed under the lowest pressure, while it occurs near the mid plane when processed under the highest pressure. Figure 5 shows that the distribution of strain rate in samples was processed under 3 GPa pressure with different numbers of turns. It shows that the strain rate changes very quickly at first and then slows down.

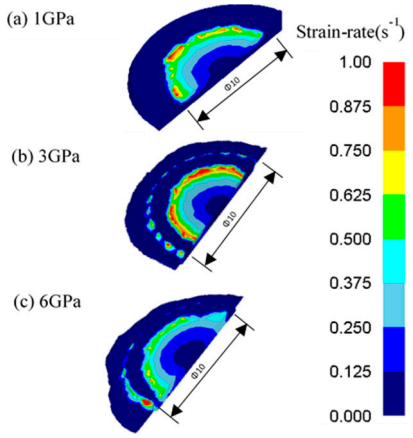


**Figure 4.** Distribution of strain rate on the half-disc surfaces and along the disc longitudinal sections for samples after a 1/2 turn with (**a**) 1 GPa; (**b**)3 GPa; and (**c**) 6 GPa.

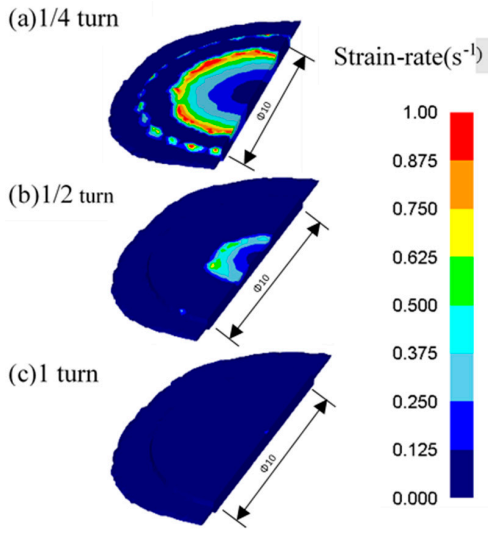


**Figure 5.** Distribution of strain-rate on the half-disc surfaces and along the disc longitudinal sections for samples with (**a**) 1/4 turn; (**b**) 1/2 turn; and (**c**) 1 turn.

### 3.1.2. The Distribution of the Effective Stress in High Pressure Torsion (HPT) Discs

The simulations showed a continuous increase in the plastic deformation imposed on the sample where the extent of the deformation is proportional to the amount of rotation which depends on the time. Figure 6 shows the distribution of the effective stress on the top surface of a sample after one half turn tested under different pressures. Separate distributions are illustrated under a pressure of 1, 3 and 6 GPa with the flow stresses illustrated pictorially using the color key shown on the right. It is apparent that the effective stress distribution is not linear. Instead, it varies significantly near the center of the disc and the variation in stress is smaller near the edge. It is also apparent that the effective stress increases with increasing pressure.

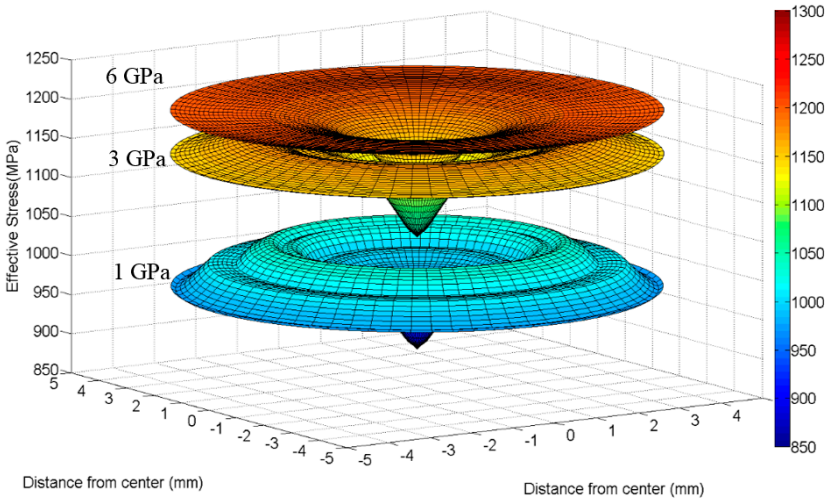


**Figure 6.** Distribution of effective stress across the disc surface after processing by HPT for a 1/2 turn under pressures of 1 GPa, 3 GPa and 6 GPa.

This trend becomes apparent in Figure 7 where the effective stress is plotted as a function of the distance from the disc center for different values of number of turns. Thus, increasing the number of turns leads to a decrease in the average compressive stresses. This reduction in the compressive stresses is due to the increase in the area of flash extruded between the anvils because this effectively

increases the area supporting the compressive load from the anvils. It is important to note that there is only a small area near the center of the disc where the compressive stresses are equal to or higher than the mean value as shown in Figure 7.

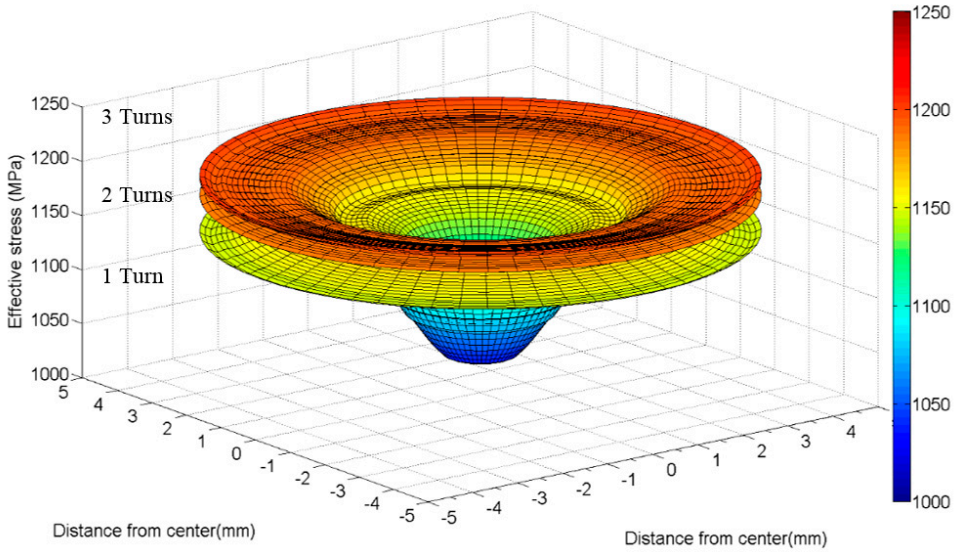


**Figure 7.** Distribution of effective stress across the disc surface after processing by HPT for 1, 2, 3 turns under 3 GPa pressure.

### 3.2. Variations in the Vickers Microhardness

Figure 8 shows the hardness profiles across the diameter of samples processed by HPT under 1, 3 and 6 GPa pressure and various number of turns. The hardness at the center of the samples does not increase with number of turns but increases with the pressure applied. With a pressure of 3 GPa, the hardness at the sample center is approximately 325 HV, while, with 6 GPa, the hardness has increased to approximately 380 HV. These values are at least 80% and 110% higher than the hardness measured in the annealed sample before HPT of 180 ± 10 HV. The hardness of all samples tended to increase at all radial positions, except the center, with number of turns, and the hardness values close to the edge of the samples were considerably harder than at the center. However, close to the sample edge, the data overlap somewhat, giving values of hardness of approximately 500 and 550 for 3 GPa and 6 GPa, respectively.

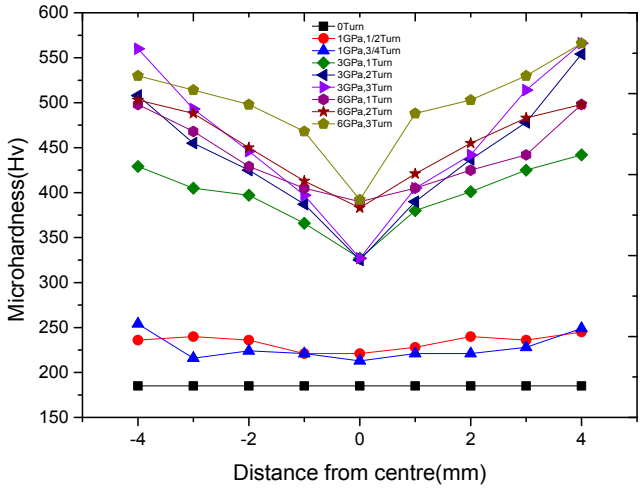


**Figure 8.** Hardness profiles after processing under 1, 3 and 6 GPa for different numbers of turns.

Figure 9 shows the overall hardness evolution of HPT discs as a function of the equivalent strain, given by Equation (1) [13], which is imposed on the disc during torsional straining. During the initial deformation in the high pressure torsion process, the hardness of the HPT discs increased almost linearly with strain from 200 to 350 HV. Subsequently, the hardness seems to increase slowly with equivalent strain. The hardness evolution with radial distance and strain for all samples is similar to the behavior registered in materials classified as being in the "without recovery" condition [14]. According to [15], Figures 8 and 9 indicate that the material has not reached the deformation conditions required to promote a homogeneous mechanical response in terms of hardness (saturation condition).

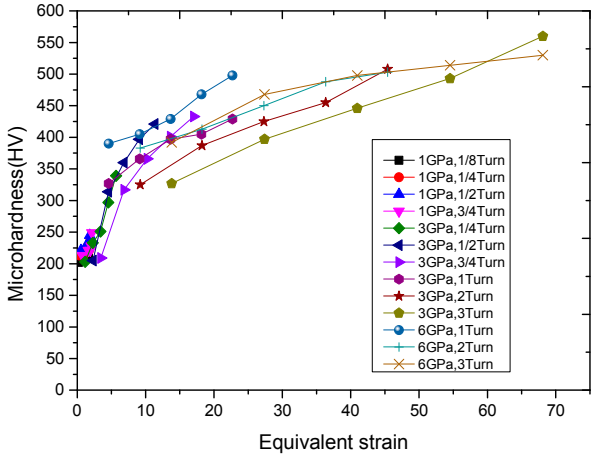


**Figure 9.** Values of the hardness plotted as a function of the equivalent strain under 1, 3 and 6 GPa for different numbers of turns.

### *3.3. Microstructures after HPT*

Figure 10 shows the changes in microstructure observed in HPT samples processed at different pressures and numbers of turns for various radial positions. All of the HPT samples showed similar features at their centers, and the microstructure is similar to the microstructure observed in the annealed steel before HPT tests (Figure 10 left column). The microstructure consisted of small, and irregular carbides distributed in a ferritic matrix. Although the microstructure looked uniform under optical microscopy, well defined carbide groups appeared in images taken using SEM/SEI, whilst other regions showed lower carbide concentrations. Some holes were detected in the sample on SEM examination, and they were created by carbides that were detached from the ferrite matrix during the grinding and polishing metallographic preparation processes.

The microstructure at regions located at 2.5 mm from the center and close to the edge shows the effects of plastic deformation revealed by the elongation of the holes left by carbide detachment and the flow patterns. However, not all of these holes appeared deformed, and only some of them changed their shape and size, suggesting that the non-uniform carbide distribution was leading to strain localisation. These variations were more marked in regions closer to the edge of the sample, and after at a greater number of turns.

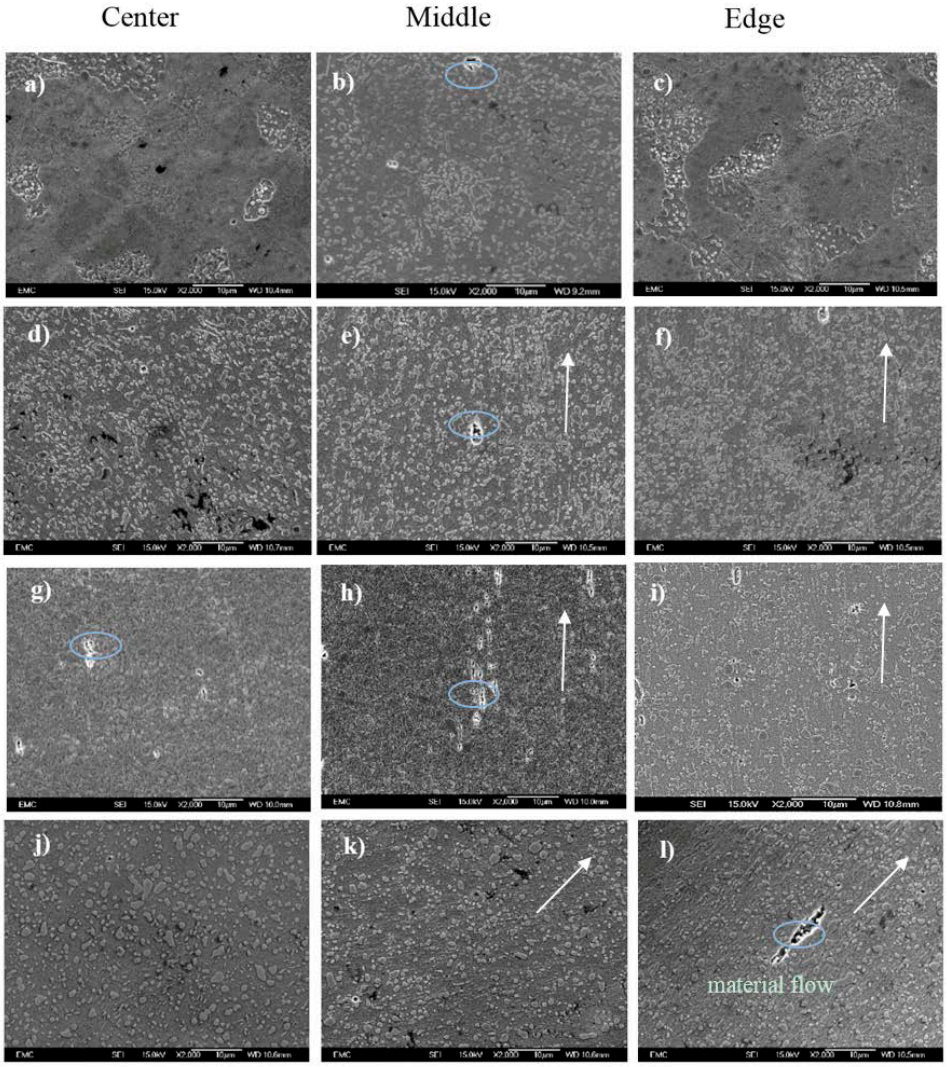


**Figure 10.** SEM showing the microstructure (**a**–**c**) at the disc center, middle and edge area in the annealed state and (**d**–**f**) after HPT processing at 3 GPa pressure with number of rotation of 1 turn, (**g**–**i**) 2 turns and (**j**–**l**) 3 turns. (The arrow indicates the shear orientation, the blue circle indicates the hole).

## 4. Discussion

### *4.1. The Evolution of the Distribution of Plastic Deformation in Samples Processed by HPT*

The present research provides a broad understanding of the distribution of plastic deformation in samples processed by HPT. The influence of different processing parameters is evaluated, and it is possible to correlate the findings both to the theory of plastic deformation and to published experimental results.

These results agree with the theoretical prediction incorporated in Equation (1) of increasing strain with increasing distance from the center of the disc. The distributions of strain are relatively similar for each simulation. It is evident that variations in pressure had no significant influence on the distributions of the effective strains. The increase in plastic deformation with distance to the center and with the number of rotations is expected to lead to an increase in strength both with increasing distance to the center and with increasing rotation, as demonstrated by the hardness results.

Plastic flow of the material has been observed in the experiment and simulation and the deformation near the mid-plane of the sample is large. It has also been reported [16–18] that the applied pressure affects the microhardness distribution on the surface of the disc. The present simulations

confirm that there are variations in the distributions of the effective stress with variations in the nominal pressure, and this becomes evident in microhardness testing.

The increase in strength with increasing distance to the disc center is in agreement with observations of increasing hardness with increasing distance to the centers of discs processed by HPT. In fact, the shapes of the curves of the distributions of strength in Figure 9 are analogous to the shapes of the curves of the distributions of hardness available in the literature [19].

### *4.2. The Evolution of the Mechanical Properties with HPT*

The present study has shown hardness at the different levels.As shown in Figure 8, the microhardness tends to increase with increasing applied pressure and number of turns, and with the distance from the center of each disc for all samples processed by HPT. The hardness at the center of the disc is lowest at 1 GPa, higher at 3 GPa and highest at 6 GPa. This confirms the trend reported earlier of gradual evolution towards homogeneity with increasing applied pressure and numbers of turns [20].

After a 1/2 turn at 3 GPa in Figure 9, the microhardness values change from 200 HV in the central region to approximately 425 HV at the edge of the disc. This type of distribution of microhardness values is in good correlation with investigations related with microhardness evolution in other metals [21,22] and is due to the variation in strain across the disc during HPT processing.

### *4.3. The Evolution of the Microstructure with HPT*

Figure 10 shows the microstructure of samples treated by HPT after different numbers of turns. It is apparent that the structure of the annealed steel after HPT is deformed, and its microstructure, characterized by spheroidized carbides and ferrite, is also clearly displayed in bright and dark contrast. At the center of the sample, the soft ferrite phase may be subdivided by dislocations after one revolution of HPT treatment [23]. This type of SPD-induced microstructural change was reported earlier in ferrite [24]. After two revolutions in Figure 10, ferrite and cementite are elongated and the spacing of the cementite precipitates has decreased somewhat. An elongated structure is expected when deformation is by a shear strain, even in the early stages of deformation [25].

Inspection of Figure 10 confirms that microstructural development in the disc has a relationship with the number of turns and the distance from the disc center (i.e., the equivalent shear strain) applied. The heavy shear strain would cause significant strength enhancement as shown in hardness evolution in Figure 10.

### *4.4. White Etching Area (WEA)*

Most importantly, it was found that WEAs similar to the butterfly wings noted in rolling contacts and cracks were formed at the edge of the samples after the HPT process at a pressure of 3 GPa, and two to three turns, as indicated in Figures 11 and 12. Plastically deformed spheroidized carbides were found in the structures. It has been previously postulated that, for a martensitic steel, the structure is composed of a dislocation cell structure and a fine granular structure, which is formed by the shear deformation of the martensite [26]. Akaoka et al. [27] reported the observation of plastic flow in a test piece with a high slip ratio along the slip direction. A similar mechanism might be applicable in this case. The results demonstrate the feasibility of using an HPT processing technique to achieve similar microstructures in the WEAs/WECs observed in rotating elements.

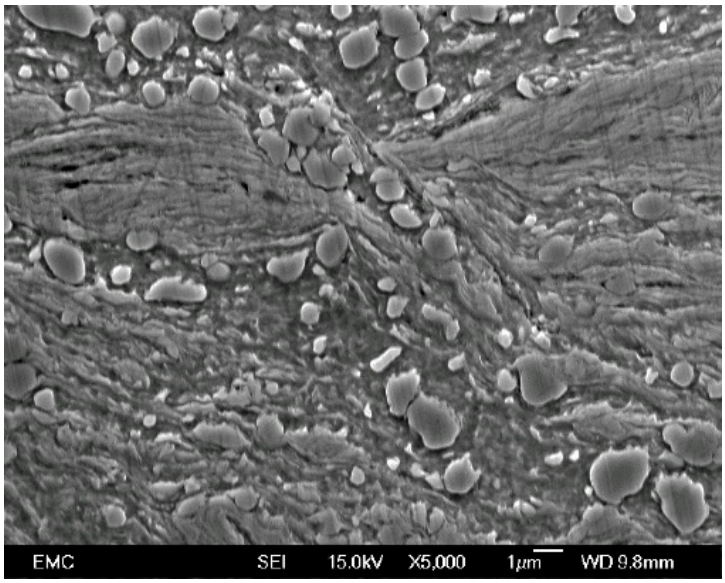


**Figure 11.** Butterfly wings in white etching areas (WEAs).

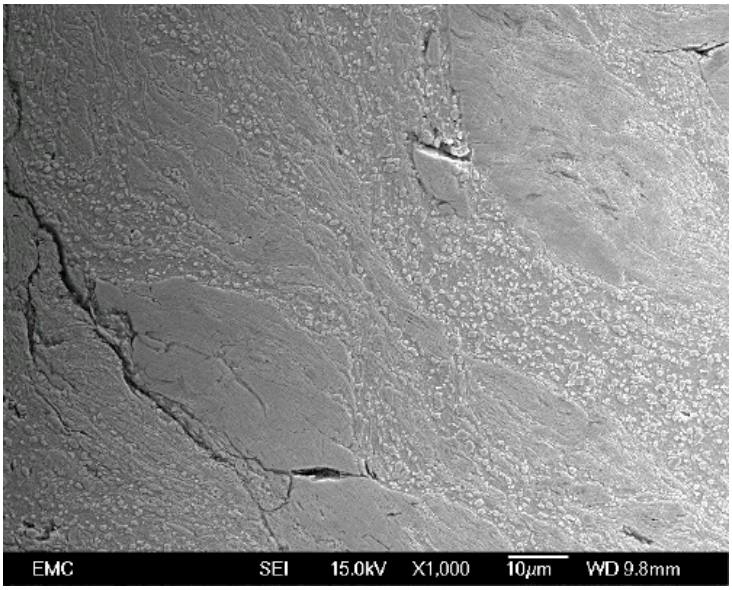


**Figure 12.** Cracks in WEAs.

## 5. Conclusions

Finite element modeling was used to examine quasi-constrained HPT processing with discs located within depressions on the inner anvil surfaces. The simulations show that the distribution of effective strain inside the quasi-constrained volume of the anvils is comparable to that predicted by ideal torsion. The applied pressure plays a minor role in the distribution of effective strain. The mean stresses during processing vary linearly with the distance to the center of the disc. Higher compressive stresses are observed in the disc center and lower stresses at the edge.

An annealed bearing steel (AISI 52100) was processed by high pressure torsion under different conditions. Microhardness measurements show the hardness increases with increasing distance from the center of the disc. Higher hardness values are attained with increasing applied pressure and/or increasing numbers of turns, but, ultimately, the hardness stabilizes in the outer regions of the discs at a value of up to three times the initial hardness in the solution-treated condition.

Structures similar to the WEAs/WECs observed in rolling elements were found at the edge of the samples processed by HPT using pressures of 3 GPa, and after two to three turns.

**Acknowledgments:** This work was supported by the National Natural Science Foundation of China (Grant No. 51405159) and the Natural Science Foundation of Shanghai (14ZR1410900). Ning Wang also thanks the financial support from the Shanghai Education Committee Foundation to visit the University of Southampton.

**Author Contributions:** This paper is a result of the full collaboration of all the authors. Ling Wang, B. G. Mellor, and Yi Huang have contributed to developing ideas, and Ning Wang and Luis V. Wilches Peña have conducted the HPT tests and subsequent analysis and carried out the analytical model. Ning Wang wrote the paper.

**Conflicts of Interest:** The authors declare no conflict of interest.

## References

1. Solano-Alvarez, W.; Bhadeshia, H.K.D.H. White-etching matter in bearing steel. Part II: Distinguishing cause and effect in bearing steel failure. *Metall. Mater. Trans. A* **2014**, *45*, 4916–4931. [CrossRef]
2. Evans, M. White structure flaking (WSF) in wind turbine gearbox bearings: Effects of 'butterflies' and white etching cracks (WECs). *Mater. Sci. Technol.* **2012**, *28*, 3–22. [CrossRef]
3. Grabulov, A.; Petrov, R.; Zandbergen, H.W. EBSD investigation of the crack initiation and TEM/FIB analyses of the microstructural changes around the cracks formed under rolling contact fatigue (RCF). *Int. J. Fatigue* **2010**, *32*, 576–583. [CrossRef]
4. Greco, A.; Sheng, S.; Keller, J.; Erdemir, A. Material wear and fatigue in wind turbine systems. *Wear* **2013**, *302*, 1583–1591. [CrossRef]
5. Valiev, R.Z.; Islamgaliev, R.K.; Alexandrov, I.V. Bulk nanostructured materials from severe plastic deformation. *Prog. Mater. Sci.* **2000**, *45*, 103–189. [CrossRef]
6. Ivanisenko, Y.; Lojkowski, W.; Valiev, R.Z.; Fecht, H.J. The mechanism of formation of nanostructure and dissolution of cementite in a pearlitic steel during high pressure torsion. *Acta Mater.* **2003**, *51*, 5555–5570. [CrossRef]
7. Langdon, T.G. Twenty-five years of ultrafine-grained materials: Achieving exceptional properties through grain refinement. *Acta Mater.* **2013**, *61*, 7035–7059. [CrossRef]
8. Pereira, P.H.R.; Figueiredo, R.B.; Cetlin, P.R.; Langdon, T.G. An examination of the elastic distortions of anvils in high-pressure torsion. *Mater. Sci. Eng. A* **2015**, *631*, 201–208. [CrossRef]
9. Kim, H.S. Finite element analysis of high pressure torsion processing. *J. Mater. Process. Technol.* **2001**, *113*, 617–621. [CrossRef]
10. Harris, T.A.; Kotzalas, M.N. *Rolling Bearing Analysis—Essential Concepts of Bearing Technology*, 5th ed.; Taylor & Francis: Boca Raton, FL, USA, 2007.
11. Sharman, K.; Bazarnik, P.; Brynk, T.; Bulutsuz, A.G.; Lewandowska, M.; Huang, Y.; Langdon, T.G. Enhancement in mechanical properties of a β-titanium alloy by high-pressure torsion. *J. Mater. Res. Technol.* **2015**, *4*, 79–83. [CrossRef]
12. Edalati, K.; Horita, Z.; Langdon, T.G. The significance of slippage in processing by high-pressure torsion. *Scr. Mater.* **2009**, *60*, 9–12. [CrossRef]
13. Zhilyaev, A.P.; Langdon, T.G. Using high-pressure torsion for metal processing: Fundamentals and applications. *Prog. Mater. Sci.* **2008**, *53*, 893–979. [CrossRef]
14. Sabbaghianrad, S.; Wongsa-Ngam, J.; Kawasaki, M.; Langdon, T.G. An examination of the saturation microstructures achieved in ultrafine-grained metals processed by high-pressure torsion. *J. Mater. Res. Technol.* **2014**, *3*, 319–326. [CrossRef]
15. Pippan, R.; Scheriau, S.; Taylor, A.; Hafok, M.; Hohenwarter, A.; Bachmaier, A. Saturation of fragmentation during severe plastic deformation. *Annu. Rev. Mater. Res.* **2010**, *40*, 319–343. [CrossRef]
16. Zhilyaev, A.P.; Nurislamova, G.V.; Kim, B.K.; Szpunar, A.; Langdon, T.G. Experimental parameters influencing grain refinement and microstructural evolution during high-pressure torsion. *Acta Mater.* **2003**, *51*, 753–765. [CrossRef]
17. Xu, C.; Horita, Z.; Langdon, T.G. The evolution of homogeneity in an aluminum alloy processed using high-pressure torsion. *Acta Mater.* **2008**, *56*, 5168–5176. [CrossRef]
18. Xu, C.; Langdon, T.G. Three-dimensional representations of hardness distributions after processing by high-pressure torsion. *Mater. Sci. Eng. A* **2009**, *503*, 71–74. [CrossRef]

19. Kawasaki, M.; Alhajeri, S.N.; Xu, C.; Langdon, T.G. The development of hardness homogeneity in pure aluminum and aluminum alloy discs processed by high-pressure torsion. *Mater. Sci. Eng. A* **2011**, *529*, 345–351. [CrossRef]
20. Zhilyaev, A.P.; Lee, S.; Nurislamova, G.V.; Valiev, R.Z.; Langdon, T.G. Microhardness and microstructural evolution in pure nickel during high-pressure torsion. *Scr. Mater.* **2001**, *44*, 2753–2758. [CrossRef]
21. Kawasaki, M.; Figueiredo, R.B.; Langdon, T.G. An investigation of hardness homogeneity throughout discs processed by high-pressure torsion. *Acta Mater.* **2011**, *59*, 308–316. [CrossRef]
22. Korznikova, E.A.; Mironov, S.Y.; Korznikov, A.V.; Zhilyaev, A.P.; Langdon, T.G. Microstructural evolution and electro-resistivity in HPT nickel. *Mater. Sci. Eng. A* **2012**, *556*, 437–445. [CrossRef]
23. Cao, Y.; Wang, Y.B.; An, X.H.; Liao, X.Z.; Kawasaki, M.; Ringer, S.P.; Langdon, T.G.; Zhu, Y.T. Concurrent microstructural evolution of ferrite and austenite in a duplex stainless steel processed by high-pressure torsion. *Acta Mater.* **2014**, *63*, 16–29. [CrossRef]
24. Song, R.; Ponge, D.; Raabe, D.; Speer, J.G.; Matlock, D.K. Overview of processing, microstructure and mechanical properties of ultrafine grained bcc steels. *Mater. Sci. Eng. A* **2006**, *441*, 1–17. [CrossRef]
25. Belyakov, A.; Kimura, Y.; Tsuzaki, K. Microstructure evolution in dual-phase stainless steel during severe deformation. *Acta Mater.* **2006**, *54*, 2521–2532. [CrossRef]
26. Oguma, N.; Harada, H.; Sakai, T. Mechanism of long life fatigue fracture induced by interior inclusion for bearing steel in rotating bending. *J. Soc. Mater. Sci. Jpn.* **2003**, *52*, 1292–1297. [CrossRef]
27. Akaoka, J.; Nitanai, A. The effect of tangential force on rolling-contact fatigue (3rd report)-influence on rolling fatigue life. *J. Jpn. Soc. Lubr. Eng.* **1982**, *27*, 268–274.